LAWRENCE
LIVERMORE
NATIONAL
LABORATORY

LLNL-JRNL-428951

Lithospheric Velocity Structure of the Anatolian plateau-Caucasus-Caspian Regions

Rengin Gok, RJ Mellors, E. Sandvol, M. Pasyanos, T. Hauk, R. Takedatsu, G. Yetirmishli, U. Teoman, N. Turkelli, T. Godoladze, Z. Javakishvirli

April 26, 2010

Journal of Geophysical Research

Disclaimer

Lithospheric Velocity Structure of the Anatolian plateau-Caucasus-Caspian Regions

R.Gök[1], R.J. Mellors[2], E. Sandvol[3], M. Pasyanos[1], T. Hauk[1], R. Takedatsu[2], G. Yetirmishli[4], U. Teoman[5], N. Turkelli[5], T. Godoladze[6], Z. Javakishvirli[6]

[1] Lawrence Livermore National Laboratory, Livermore, CA, USA

[2] San Diego State University, San Diego, CA, USA

[3] University of Missouri, Columbia, MO, USA

[4] Republic Seismic Survey Center, Azerbaijan

[5] Kandilli Observatory and Earthquake Research Institute, Cengelkoy, Istanbul,Turkey

[6] Seismic Monitoring Center, Georgia

Abstract

The Anatolian Plateau-Caucasus-Caspian region is an area of complex lithospheric structure accompanied by large variations in seismic wave velocities. Despite the complexity of the region little is known about the detailed lithospheric structure. Using data from 31 new permanent broadband seismic stations along with results from a previous 29 temporary stations and three existing global seismic stations in the region, a 3D velocity model is developed using joint inversion of teleseismic receiver functions and surface waves. Love and Rayleigh surface waves group and phase dispersion curves were derived from regional and teleseismic events. Additional surface wave group dispersion curves were determined using ambient-noise correlation. These dispersion curves were included in global inversion. Receiver functions were calculated using teleseismic P arrivals from 789 teleseismic earthquakes. The stacked receiver functions and surface wave dispersion curves were jointly inverted to yield the absolute shear wave velocity to a depth of 100 km at each station. The depth of major discontinuities (sediment/basement, crust/mantle, and lithosphere/aesthenosphere) inferred from the velocity/depth profiles at the location of each station. Distinct spatial variations in crustal and upper mantle shear velocities were observed. The Kura basin showed slow (~2.7-2.9 km/s) upper crustal (0-11 km) velocities but elevated (~3.8-3.9 km/s) velocities in the lower crust. The Anatolian plateau varied from ~3.1 - 3.2 in the upper crust to ~3.5-3.7 in the lower crust while velocities in the Arabian plate (south of the Bitlis suture) were slightly faster (upper crust between 3.3 - 3.4 and lower crust between 3.8-3.9 km/s. The depth of Moho, which was estimated from the shear velocity profiles, varied from 35 km in the Arabian plate and increased northward to 54 km at the southern edge of the Greater Caucasus. Moho depths in the Kura and at the edge of the Caspian showed more spatial variability but ranged between 35-45 km. Upper mantle velocities were slow under the Anatolian plateau but increased to the south under the Arabian plate and to the east (4.3-4.4) under the Kura basin and Greater Caucasus. The areas of slow mantle coincided with the locations of Holocene volcanoes. Differences between Rayleigh and Love dispersion at long wavelengths a pronounced variation in anisotropy between the Anatolian plateau and the Kura basin.

Introduction

The continental collision zone between the Arabian and Eurasian plates has led to formation of 2 km high plateau and the formation of a diffuse zone of deformation that extends from the Bitlis suture to the Greater Caucasus (Figure 1). In addition to the fold and thrust belts typical of most continental collision zones, the Arabia/Eurasia transition zone includes the South Caspian basin, a 20 km deep sedimentary basin of uncertain origin (Sengor, 1990; Brunet et al., 2003; Khain, 2005) and the Anatolian-Iranian plateau, an uplifted volcanic area dominated by active strike-slip faults in eastern Anatolian and the Lesser Caucasus and thrust faults in the Zagros mountains (Barazangi et al., 2006; Gogus and Pyshlywec, 2008; Ershov and Nikishin, 2004; Maggi and Priestley, 2005). Explanations of this diversity in tectonic styles differ but generally invoke subduction (and/or delamination) episodes embedded within the collision zone (Priestley et al., 1994; Sengor, 2003; Masson et al., 2006; Gogus and Pysklywec, 2008). Contributing to the poor understanding is the lack of a comprehensive crustal and lithospheric velocity model of the region. Large-scale regional and global models (e.g. Bijward et al., 1998; Piromallo and Morelli, 2003) show intriguing features but cannot resolve the fine details. In the Caucasus region much of the detailed information on crustal and upper mantle velocity structure is based on refraction data collected in the 1960's (e.g. Neprochov, 1968) along with data from a few temporary deployments and sparse global seismic stations (Mangino and Priestley,1998). More recent data (e.g. Sandvol et al., 2003) collected in the Anatolian plateau have image the bulk lithospheric structure of eastern Anatolia but the transitions between the plateau and the surrounding tectonic units are unclear. A comprehensive velocity model would aid in the understanding of this complex region. A detailed model is also essential in mapping regional wave propagation and improving the accuracy of earthquake hypocenters throughout the region.

This paper presents a model of the crustal and upper mantle structure of the Anatolian plateau/Caucasus/Caspian region using waveform data from 31 new broadband stations in the region (Figure 1) combined with previous data. The new broadband stations are part of the Azerbaijan, Georgian, and Turkish national seismic networks. The spatial coverage of this dataset

represents a significant improvement over previously available broadband data, which was restricted to three global stations and a few temporary deployments. In this study, we combine surface waves with receiver functions to obtain a constrained shear wave velocity model of the crust and upper mantle to a depth of 100 km. The results provide a comprehensive view of the crustal structure and illuminate the transitions between the various tectonic units.

Geologic and tectonic setting. A broad zone of deformation exists along the northern edge of the Arabian Plate and extends from the Zagros Mountains to the Caucasus/Caspian region. The current style of deformation varies from compression and thrusting in the Zagros to strike-slip in the Anatolian plateau (Allen et al., 2004). As the Arabian plate is moving northward with respect to Eurasia at a rate of approximately 18 mm/year (Reilinger et al, 2006), the deformation zone has generally been attributed to the ongoing continental collision (Dewey and Sengor, 1979) but other mechanisms such as orogenic collapse or slab pull may play a significant role (Allen et al., 2004; Vernant and Chery, 2006). Prior to the present configuration, active subduction of the Neo-Tethys oceanic lithosphere occurred along the northern edge of the Arabian plate. This subduction ceased approximately 24 Ma at the beginning of the Miocene as all oceanic crust was consumed (Sengor et al., 2003) although the timing varies substantially along the Eurasian-Arabian plate boundary. The continued Arabian/Eurasia convergence has affected the Anatolian plateau, the Caucasus, and the South Caspian basin in distinctly different fashions.

The most prominent feature in the area of interest is the South Caspian Basin, a deep (~ 20km) sedimentary basin filled with mostly Pliocene-Quaternary sediments (Knapp et al., 2000; Allen et al; Brunet et al, 2003). The exact origin and age of the South Caspian is uncertain. Brunet et al. (2003) suggests that it is a backarc basin which underwent increased subsidence at the onset of continental collision (Brunet et al., 2003). Other possibilities include remnant oceanic crust (Nadirov et al., 1997) or a large-scale pull-apart basin (Sengor, 1990). The basin is bordered by thrust faults on the west, south, and east (Allen et al., 2002) but internally the basin remains relatively undeformed. The northern edge is marked by a large anticline, the Absheron megastructure, which cuts northwest-southeast across the Caspian Sea. The Absheron structure coincides with a northwest-southeast belt of seismicity including moderate depth (as deep as 70 km) earthquakes that occur at the northern edge of the south Caspian Sea basin. This seismicity (Priestley et al., 1994) as well as gravity (Allen et al., 2002) and deep seismic reflection data (Knapp et al., 2000) suggest that the

South Caspian crust is subducting northward under the Eurasia plate along this zone. It is unclear how far the subduction extends to the west. Estimates of the initiation of the subduction range from 2 to 10 Ma. (Hollingsworth et al., 2008). Refraction lines and onshore receiver functions indicate a thin but high-velocity crust suggesting either remnant oceanic crust or thinned continental crust (Neprochov, 1968; Mangino and Priestley, 1998). Lg is blocked but Sn propagates well (Kadinsky-Cade et al., 1981; Rodgers et al., 1997; Gök et al, 2003). Pn velocities are normal or possibly slightly elevated (e.g. 8.0-8.2 km/s)(Hearn and Ni, 1994; Al-Lazki et al, 2003; Toksoz et al., 2006) . The thick upper package of low-velocity sediments is well-documented by reflection seismic data and has a profound effect on surface Rayleigh wave propagation at frequencies of 25-50 seconds (Priestley et al., 2001).

Between the South Caspian and the Black Sea a complex area lies containing the Greater Caucasus and the associated Kura Basin. The Greater Caucasus are primarily a fold and thrust belt and represent the northern extent of significant deformation between the Arabian and Eurasian plates. GPS data shows about 7 to 14 mm/yr of shortening across the Greater Caucasus (Reilinger et al. 2006; Masson et al., 2006). This has been interpreted to suggest that subduction may be continuing under the Greater Caucasus (Vernant and Chery, 2006). The western Greater Caucasus includes several Holocene volcanic areas and gravity data indicates a decrease in lithospheric strength from east to west (Ruppel and McNutt, 1990). Sn also appears to suffer greater attenuation in the western Greater Caucasus than in the eastern section. Refraction data indicate a crustal thickness of approximately 50-55 km with moderate to low crustal velocities (Ershov et al., 2003).

South of the Greater Caucasus and bordering the South Caspian basin is the Kura Basin, a lowland with up to 15 km of sediments (Brunet et al. 2003) and inferred to be a foreland basin to both the Greater and Lesser Caucasus. Structurally, it is separated from the South Caspian basin by a ridge of uplifted basement (the Talysh-Vandam basement high) and the inferred West Caspian fault (Kadirov and Askerhanova, 1998). Refraction data indicate a high velocity lower crust in places (Ershov et al., 2003). A well drilled to a depth of 8.3 km on the Talysh-Vandam basement high showed 2-3 km of sediments over metamophosed volcanics. On the east side of the basement high the sediments thicken greatly into the South Caspian. The Kura Basin is bordered on the southeast by the thrust faults of the Talysh Mountains and on the southwest by the Lesser Caucasus. Regional wave propagation and velocities are poorly constrained in this region but it appears that high Pn and

Sn velocities extend into the Kura basin from the South Caspian but that Sn may be attenuated in the western Greater Caucasus (Martin et al., 2008).

The Turkish/Iranian plateau is an uplifted volcanic plateau (Barazangi et al., 2006; Maggi and Priestley, 2005) with an average crustal thickness of 40-50 km that increase from south to north. Low Pn velocities (7.6 km/s), highly attenuated Sn, and receiver functions indicates that the lithospheric mantle is thin or missing (Gok et al., 2003; Zor et al., 2003; Al-Lazki et al., 2004; Angus et al., 2006) and therefore elevations are supported by buoyant asthenosphere rather than thickened crust (Sengor et al., 2003). The abnormally hot upper mantle and widespread volcanics may be related to the detachment of the subducting slab or continental delamination about 11 Ma. Detailed receiver functions and resistivity measurements indicate that the possible delaminated lithospheric fragments possess a complex geometry (Ozacar et al., 2008; Turkoglu et al., 2008). An alternate possibility is that remnant water and fluids from the subducting oceanic slab may be affecting mantle properties (Hearn and Ni, 1994; Maggi and Priestley, 2005), although the chemistry of the volcanic rocks is not consistent with this interpretation.

In general, while the individual structure of each tectonic unit is fairly well understood the interaction between units and transitional structure is poorly defined. This paper seeks to provide a clear and comprehensive model of the area.

Data

Recently, permanent broadband stations have been deployed across the Caucasus and eastern Turkey region as part of various national networks (Azerbaijan(14), Georgia(4) and Turkey(13)) providing an excellent opportunity to study the lithospheric structure. We used data from 31 newly available broad-band stations that have been installed in recent years (Figure 1). These stations are part of the Azerbaijan National Seismic network, the Georgian Seismic Network, and stations run by Kandilli Observatory in Turkey. The Azeri stations are STS-2 seismometers (0.02 to 50 Hz) and the Kandilli and Georgian network are a mix of CMG-3ESP, CMG-3T and CMG-40T. To accompany this data set waveform data was also collected from 2005 to 2009 for the relevant global seismic stations (GNI, ABKT, and KIV).

Method

The combination of receiver functions and surface waves is a powerful method to infer crustal and upper mantle shear wave velocities. Receiver functions isolate the response of near vertically propagating plane waves to seismic velocity discontinuities under a seismic station and are primarily sensitive to the depth of velocity contrasts but have poor sensitivity to absolute velocities. Surface wave dispersion is primarily controlled by the S-wave velocity structure but possesses poor sensitivity to velocity discontinuities or fine structure. Therefore, inverting both surface wave dispersion and receiver functions simultaneously should improve the reliability of the results (Julia et al., 2000).

Receiver Functions

Tele-seismic events between 30 and 90 degrees with a magnitude greater than Mb=5.5 were extracted from the data and receiver functions were calculated for all stations. Due to varying data availability, the largest number of events was recorded by the GSN stations with over 600 candidate events. Most of the other stations possessed between 100 and 200 candidate events. Azimuthal coverage was excellent to the east but poorer toward the west (Figure 2). The time domain iterative deconvolution of Ligorria and Ammon (1999) was used to calculate the receiver functions with a Gaussian filter (a) of 1.0, 1.5 and 2.5 seconds. All events and receiver functions were visually inspected for high signal to noise and only results with a high signal to noise were used.

The quality of the receiver functions was poor for several of the Azerbaijan stations due to high noise levels (especially NDR, GOB, and GAL) and thick sedimentary layers under most stations, which produced pronounced multiples. Figure 2 shows the radial component receiver functions for all events at selected, characteristic stations plotted as a function of backazimuth. Because of the limited space here we will be discussing only these selected stations. Very strong crustal multiples are observed at stations BRD, QUB and IML. QUB is located at the northern edge of the Greater Caucasus (Figure 1) where several layers of multiples that cause very broadened P waveforms with multiples. LKR, located at the boundary between Talysh mountains and the Kura basin, displays a clear consistent Ps_{MOHO}. Mangino and Priestley (1998) found 33 km thick crust for station LNK (co-located with LKR) with 13-km-thick sedimentary section lying on a high-velocity lower-crustal section using only receiver functions. Variations in receiver functions waveforms with

backazimuth and significant energy on the tangential components suggest important lateral variations in structure under several stations as well (e.g. QUB, MTDA, LKR on Figure 2). In general, the stations in eastern Turkey showed clearer results although CUKT, located at the Bitlis-Zagros fold and thrust belt, has a slightly noisier and incoherent signal combined with low amplitude Ps_{MOHO}. We initially used forward modeling and the slant stack technique of Zhu and Kanamori (2000) to estimate Moho depth and crustal properties (Takedatsu et al., 2008) but the strong multiples present in the receiver functions added considerable error in the estimates and we prefer using the additional constraints provided by the joint inversion.

Surface Wave Analysis

Several methods were used to obtain surface wave dispersion curves. These included event-based methods used for both group and phase velocities as well as Rayleigh wave group dispersion estimate from ambient noise cross-correlation. The dispersion curves generated for each station pair were then spatially interpolated to extract the best-fit dispersion curves over a set of spatial grid points although different algorithms were used to determine group and phase dispersion.

We calculated the Love and Rayleigh wave group velocity dispersion curves of over 1500 waveforms (7-90 sec) at distances of 0-90 degrees. Waveforms were filtered and dispersion curves manually picked using the multiple frequency implementation. The horizontal components showed higher noise levels than the vertical component and hence the dispersion curves for Love waves have higher errors than the corresponding Rayleigh dispersion curves especially at longer (more than 70 seconds) periods. Ambient noise correlation with sign-bit normalization was applied to 406 station pairs to obtain Rayleigh wave group velocities. Figure 3a shows the Green's functions obtained by cross-correlating 1 hour segments of vertical component data from station GNI with all other stations, stacking, and then filtering at 20-50 sec. Again, due to variation in available data the amount of inter-station overlap varied but the shortest period of inter-station overlap was 90 days.

Group velocity dispersion curves from all station-event and station-station (ambient-noise) correlations were inverted using the global/regional surface wave tomography algorithm of Pasyanos (2005). The inversion also includes measurements from other stations in the region. This method generates an interpolated dispersion curve over a set of spatial grid points (0.5°x0.5°). The group velocity dispersion curves appropriate for each station were then extracted from the tomographic inversion maps. Results from three stations (in the Kura Basin, Anatolian Plateau, and

Greater Caucasus) are shown in Figure 3b. Anatolian plateau is significantly lower at longer periods. Kura and Greater Caucasus is low at short periods where crust is overlaid by thick sediments.

The phase velocity map was obtained with the method of Yang and Forsyth et al., (2003) at periods between 20-145 seconds. Initially, a 1-D fit to all data was estimated and then phase velocities were inverted in 50km spacing at 13 different frequencies using the 1D fit as a starting model. As in group velocities, Rayleigh wave individual station dispersion curves to be used at joint inversion were also extracted from the 2-D phase velocity tomography results (Skolebletseyn et al., 2009).

Inspection of the phase and group velocity maps showed trends consistent with the known surface geology. Compared to Kura and Greater Caucasus, we observe lower velocities below the eastern Anatolian Plateau above 45 seconds. Highest velocities in the upper mantle are observed in the Greater Caucasus, while the slowest velocities at short periods (10-30 sec) are observed both Greater Caucasus and Kura basin which reflects the slow, thick sediments of the region.

Joint Inversion

The stacked radial receiver functions (Gaussian filtered at 1.0, 1.5, and 2.5 seconds) and the interpolated dispersion curves (Rayleigh (group+phase), Love (group)) for each station are inverted to yield a 1D shear wave model to a depth of 100 km at each station location. The method of Julia et al. (2000) is used. In brief, an iterative, damped, least-squares algorithm is applied to find the best-fitting model that fits both the observed receiver functions and the dispersion curves. Important adjustable parameters are the starting model, the smoothing between adjacent vertical layers, and the relative weighting between the datasets (receiver functions and surface waves). Additional details can be found in Julia et al., (2000; 2003) and the reader is advised to consult those for further details.

Initially, a simplified continental model was used based on the combined IASPEI91 and AK135 global models. For stations in the Kura Basin region the inversion did not converge and a thick, low-velocity sedimentary layer was added to the starting model in accordance with the known structure of the region based on deep drillholes, surface geology, and a variety of geophysical studies (e.g. Kadirov and Askerhanova, 1998l). We basically replaced the uppermost crustal layer with 10 km of low velocity, sedimentary layer (Figure 4, blue line). Three different weighting schemes were

tested (30-70%; 50/50%; and 70/30%) to weight the receiver function and surface wave misfit, respectively. We fixed smoothness parameter (Julia 2000, equation 6) to 0.6 during inversion. In most cases, velocity profiles for all three relative weights were similar except at shallow (< 10 km) depths. Figure 4 shows an example of the joint inversion data and results for station QUB. A 1-D velocity profile was obtained for each station as it is shown at the figure. We started with the initial model (blue line) and used three different weights to obtain the average model that would best represent the structure below that station. Red lines are individual synthetic receiver functions after each inversion, black line at the right panel is the average of all models.

Results and Conclusion

Inversion results are shown in Figures 5 and 6. We combined the 31 new measurements with results from a previous 29 station temporary deployment on the Anatolian plateau processed using similar methods from Gök et al., (2006).

Moho depths were estimated from the shear wave profiles resulting from the shear wave profiles by inspecting profiles for large gradient change and reaching the value of 4.2 km/s. This value of Vs is slower that any upper mantle velocity value. However the smoothness factor in the inversion and the gradients in Figure 5 shows the resulting map derived by interpolating the Moho depth estimates at each station using a neighborhood algorithm (at distance of 200 km). These estimates were compared with estimates of Moho depths obtained using receiver functions alone with a slant-stacking technique of Takedatsu et al., 2009. We observed larger differences at two methods of thicknesses at thick sedimentary basin stations (ALI, IML, BRD, QUB, SIZ). The Lesser Caucasus has the thickest crust (~52 km), which is thinner than the estimate of Sandvol et al (1998). Coverage of the Greater Caucasus was sparse, but suggests 50 km in the west and 45-50 in the east. The Kura/South Caspian showed mixed results, possibly due to poor resolution by the receiver functions related to multiples within the upper crust. The Arabian plate showed the most homogenous results with thickness of 35 km.

Horizontal depth slices of 10, 35 and 85 km are shown in Figure 6. The thick sediments of Kura Basin is still observed with low velocities with the average Vs=2.8 km/s at 10 km slice. The eastern part of the Greater Caucasus shows similar low velocities in the upper crust. The northern part of mountains is also overlain by relatively young Oligocene to Quaternary sediments. The slowest lower crustal velocities are observed in the northeastern Anatolian plateau and Lesser

Caucasus region where the intensified Neogene/Quaternary, Holocene volcanoes were observed (Figure 6, 35 km depth). Gök et al, (2000) noted severe attenuation within the crust where the shear velocities were eliminated at 90-100km epicentral distances.

There were cases where we observed the discrepancy between Love and Rayleigh wave simultaneous inversion. Love waves are sensitive to the velocity of horizontally propagating SH waves while the receiver functions and Rayleigh waves are sensitive to the vertically propagating SV waves. The inability to fit data in the long period portion of the dispersion curves may indicate the existence of the radial anisotropy in the upper mantle. To test the existence of anisotropy we performed two separate inversions with individual Love and Rayleigh wave inversions. The results are shown in Figure 6. At 57 and 85 km depth, where the lithospheric mantle is present the vertically polarized S wave travels faster than the horizontally polarized S wave (SV > SH). This feature is observed in the Greater Caucasus and Kura but not observed under the Anatolian plateau and Lesser Caucasus between the depths of 57-100km (Figure 6). We observe slower S-wave velocities throughout the plateau, northern Arabian plate, Lesser Caucasus as well as SH being higher (4-8 %) than SV. SH > SV in the asthenosphere might be related to the shear flow with a significant horizontal component. If it is the case we might consider this as the boundary of lithosphere. The lithosphere is possibly slightly deeper (see the boundary in Figure 6).

The slowest crust and upper mantle velocities are observed in Lesser Caucasus progressing from south to north (Figures 6). A clear, relatively fast shear velocities feature apparent in the improved Caucasus model is relatively fast shear velocities within Kura Basin and Greater Caucasus. There is little change in the magnitude of velocity estimates across much of the Lesser Caucasus along transects perpendicular to the Caucasus.

Regional waves propagating in the crust (Lg) is sensitive to crustal thickness variations and the upper mantle (Sn) is greatly affected by the upper mantle velocities. The presence of Sn is an indication of a stable and relatively thick lithospheric mantle. To test the validity of our velocity model we inspected regional waveforms for simply checking the presence of Sn and Lg. We show an example, a magnitude 5.1 event occurred at northern part of Greater Caucasus recorded by most of our stations (Figure 7a). We show paths from event to station if Sn is present and clearly observed within 0.5-8 Hz pass-band. Both Lg and Sn completely disappear when they travel through the Anatolian plateau. Within Kura and part of the greater Caucasus Sn is very prominent phase. We used the visually inspected waveforms following the technique of Sandvol et al., for Sn

efficiency tomography map. We added our observations to the existing Sandvol et al., (2000) and Gok et al., (2001, 2003). Figure 7b shows Sn propagation efficiency map of the region. The region with very low S-wave velocities (patched at figure) at 85 kilometers and the presence of seismic transverse isotropy (SH>SV) generally coincides with the zones of inefficient Sn propagation.

Discussion

Crustal thickness patterns suggest the majority of crustal thickening has occurred far from the Arabian-Eurasian plate boundary along the Pontides and Greater Caucasus. This first suggests that there has been limited crustal thickening exempt in the northern portion of the collisional belt between Arabia and Eurasia. This thickening seems to have occurred against the strong rigid lithosphere of the Black Sea and Siberian craton that may have acted as a backstop to the weaker lithosphere of the Anatolian plateau and Lesser Caucasus. Given the low crustal shear velocities and the pervasive volcanism in the Eurasian crust just north of the Bitlis suture it seems unlikely that this was accomplished by transmitting stress from the plate boundary to the northern Pontides and Greater Caucasus. This crustal thickening might have occurred during the last stages of subduction of the NeoTethys when there was possibly a flat slab subduction below the Anatolian plateau (Barazangi et al., 2006). This would also be consistent with the idea that there was only significant crustal shortening prior to the development of continental escape and the associate northern and eastern Anatolian fault zones.

We also observe possible crustal melt zones with extremely low velocities in the mid to lower crust in easternmost Anatolia and the western Lesser Caucasus. Overall this zone seems to coincide with the location of active volcanism but thinner crust. This suggest that these low velocities and possible crustal melt zones are produced from heating associate with a thin to absent mantle lid as opposed to the accumulation of large amounts of radiogenic material in a thickened crust. This is also consistent with the lack of crustal thickening that we observe in the eastern Anatolian plateau. Our map of the thinnest lithosphere is limited to eastern Anatolia and does not extend into the Lesser Caucasus, Kura basin, or Greater Caucasus. This is consistent with the idea of a slab-break off or delamination event occurring close to the Arabian-Eurasian plate boundary. However the lack of crustal thickening in the regions of thinner lithosphere seem to argue for slab break off rather than delamination.

Acknowledgements

We would like to thank our Turkish, Azeri and Georgian collaborators for their hospitality during our trips to the region. We like to thank Rob Reilinger and Keith Priestley for discussions about the region. Special thanks to Nancy McGee for her insightful contribution. This project is funded by Air Force Research Laboratory contract number xxxxxxx. This project was supported by the Lawrence Livermore National Laboratory under the auspices of the U.S. Department of Energy by Lawrence Livermore National Laboratory under Contract DE-AC52-07NA27344. This is LLNL contribution LLNL-JRNL-XXXX

REFERENCES

Al-Lazki et al., 2003 A.I. Al-Lazki, D. Seber, E. Sandvol, N. Turkelli, R. Mohamad and M. Barazangi, Tomographic Pn velocity and anisotropy structure beneath the Anatolian plateau (eastern Turkey) and the surrounding regions, *Geophys. Res. Lett.* 30 (24) (2003), p. 8043.

Al-Lazki et al., 2004 A.I. Al-Lazki, E. Sandvol, D. Seber, M. Barazangi, N. Turkelli and R. Mohamad, On tomographic imaging of mantle lid velocity and anisotropy at the junction of the Arabian, Eurasian and African Plates, *Geophys. J. Int.* 158 (2004), pp. 1024–1040

Allen, M., Jackson, J. & Walker, R., 2004. Late Cenozoic reorganization of the Arabia-Eurasia collision and the comparison of short-term and long-term deformation rates, Tectonics, 23, TC2008, doi:10.1029/2003TC001530.astr. Soc., 77, 185264.

Baumgardt, D. R. (2001). Sedimentary basins and the blockage of Lg wave propagation in the continents, Pure and Appl. Geoph., 158, 1207-1250.

Bijwaard, H., Spakman, W. and Engdahl, E.R., 1998. Closing the gap between regional and global travel time tomography. *Journal of Geophysical Research* 103, pp. 30055–30078.

Bostock, 1999 M.G. Bostock, Seismic waves converted from velocity gradient anomalies in the Earth's upper mantle, *Geophys. J. Int.* 138 (1999), pp. 747–756.

Brunet, M.F., M. V. Korotaev, A. V. Ershov, and A. M. Nikishin (2003). The South Caspian Basin; a review of its evolution from subsidence modeling, Sedimentary Geology, 156, 1-4, 119-148.

Dewey and Şengör, 1979 J.F. Dewey and A.M.C. Şengör, Aegean and surrounding regions: complex and multiplate continuum tectonics in a convergent zone, *Geological Society of America Bulletin* 90 (1979), pp. 84–92.

Ershov M, Saxena S, Karbasi H, Winters S, Minehane S, Babcock J, et al. Dynamic recovery of negative bias temperature instability in p-type metal–oxide–semiconductor field-effect transistors. Appl Phys Lett 2003;83(8): 1647–9.

Ershov, A. V. & Nikishin, A. M. (2004). Recent geodynamics of the Caucasus^Arabia^East Africa region. Geotectonics 38, 123-136.

Forsyth, D.W., Webb, S.C., Dorman, L.M., Shen, Y. (1998). Phase velocities of Rayleigh waves in the MELT experiment on the East Pacific Rise. Science, 280, 1235-1238.

Gögüs and Pysklywec, 2008 O.H. Gögüs and R.N. Pysklywec, Mantle lithosphere delamination driving plateau uplift and synconvergent extension in eastern Anatolia, *Geology* 36 (2008), pp. 723–726.

Gök, R., M.E. Pasyanos and E. Zor (2006), Lithospheric Structure of the Continent-Continent Collision Zone: Eastern Turkey, submitted to J. Geophys. Res.

Gök R.,E. Sandvol,N. Türkelli, D. Seber and M. Barazangi,(2003), Sn attenuation in the Anatolian and Iranian plateau and surrounding regions, Geophys. Res. Lett., 30, 24, 8042

Gök, R., N. Turkelli, E. Sandvol, D. Seber and M. Barazangi, (2000). Regional wave propagation in Turkey and surrounding regions, Geophys. Res. Let., 27, 3, 429-432.

Hearn, T. and J. Ni (1994). Pn velocities beneath continental collision zones: the Turkish-Iranian plateau, *Geophys. J. Int.* 117, 273-283.

Jackson J., Priestley, K., Allen, M., and Berberian, M., (2002), Active tectonics of the South Caspian Basin: Geophysical Journal International, v. 148, p. 214–245.

Julia, J., C. Ammon, R. Herrman, and A. Correig, (2000). Joint inversion of receiver function and surface wave dispersion observations, Geophys. Jour. Int., 143,1, 99-112.

Kadinsky-Cade, K., Barazangi, M., Oliver, J. and Isacks, B.(1981). Lateral variations of high-frequency seismic wave propagations at regional distances across the Turkish and Iranian plateaus, J. Geophys. Res., 86, 9377–9396.

Kadirov, F., Askerhanova, N., (1998). Gravity Model of the Hekery- Rive-Fuzuli-Carli-Maraza (Azerbaijan) Profile. EAGE, Leipzig,p. 7.

Knapp, C. C., J. H. Knapp, and John A. Connor, Crustal-Scale Structure of the South Caspian Basin Revealed by Deep Seismic Reflection Profiling, Marine and Petroleum Geology, 21, 1073–1081, 2004

Laske, G. and G. Masters, (1997). A Global Digital Map of Sediment Thickness, EOS Trans. AGU, 78, F483.

Ligorria, J. P., and C. J. Ammon (1999), Iterative deconvolution and receiver-function estimation, *Bull. Seismol. Soc. Am.*, *89*, 1395–1400.

Maggi A., K. Priestley, 2005. Surface waveform tomography of the Turkish-Iranian Plateau. Geophysical Journal International, 160, 1068-1080.

Mangino, S and K. Priestley, (1998). The crustal structure of the southern Caspian region, Geophys. Jour. Inter., 133,(3),630-648Martin, R. M. L. Krasovec, S. Romer, M. N. Toksöz, S. Kuleli, L. Gulen, and E. S. Vergino (2005), The Caucasus seismic information network study and its extension into Central Asia, 27th Seismic Research Review: Ground-Based Nuclear Explosion Monitoring Technologies, Sept. 20-22, Rancho Mirage, CA.

Masson, F., Djamour, Y., Vangorp, S., Chéry, J., Tavakoli, F., Tatar M. & Nankali, H., 2006. Extension in NW Iran inferred from GPS enlightens the behavior of the south Caspian basin, *EPSL,* 252, 180–188.

Mitchell, B., Lg coda Q variation across Eurasia and its relation to crustal evolution, (1997). J. Geophys. Res 102, (10), 22,767-22,779

Ozacar, A.A., Gilbert, H., and Zandt, G., (2008), Upper mantle discontinuity structure beneath East Anatolian Plateau (Turkey) from receiver functions: Earth and Planetary Science Letters, v. 269, p. 427–435.

Pasyanos M.E., A variable resolution surface wave dispersion study of Eurasia, North Africa, and surrounding regions, (2005). J. Geophys. Res., 110, B12301, doi: 10.1029/2005JB003749.

Priestley, K., H. Patton, and C. Schultz (2001), Modeling anomalous surface-wave propagation across the southern Caspian Basin, Bull. Seismo. Soc. Amer., 91, (6), 1924-1929.

Reilinger, R., et al. (2006), GPS constraints on continental deformation in the Africa-Arabia-Eurasia continental collision zone and implications for the dynamics of plate interactions, *J. Geophys. Res.*, 111, B05411, doi:10.1029/2005JB004051.

Rodgers, A. J., J. F. Ni, T. M. Hearn, (1997). Propagation characteristics of short-period Sn and Lg in the Middle East, Bull. Seismo. Soc. Amer., 87, (2), 396-413.

Ruppel, C., and M. McNutt (1990), Regional compensation of the Greater Caucasus mountains based on an analysis of Bouguer gravity data, *Earth Planet. Sci. Lett.*, *98*, 360–379.

Sandvol, E., K. Al-Damegh, A. Calvert, D. Seber, M. Barazangi, Mohamad, R, R. Gök, N. Turkelli, and C. Gurbuz, (2001). Tomographic imaging of Lg and Sn propagation in the Middle East, Pure and Applied Geophysics, 158, 1121-1163.

Sandvol, E., Turkelli, N., and Barazangi, M., The Eastern Turkey Seismic Experiment: The study of a young continent-continent collision, Geophysical Research Letters, 30, 8038, doi:10.1029/2003GL018912, 2003.

Sengor et al., 2003 A.M.C. Sengor, S. Ozeren, T. Genc and E. Zor, East Anatolian high plateau as a mantle-supported, north–south shortened domal structure, *Geophys. Res. Lett.* 30 (24) (2003), p. 8045.

Toksoz, M, Y. Sun, C. Li, R. van der Hilst and D. Kalafat (2006), Seismic Tomography of the Arabian-Eurasian collision zone and tectonic Implications, Eos Trans. AGU, 89(53), **Fall Meet. Suppl.,** #T23D-01.

Vernant, P. Chéry, J., 2006. Mechanical modelling of oblique convergence in the Zagros, Iran, *Geophys. J. Int.* , 165 , 991–1002.

Zor et al., 2003 E. Zor, E. Sandvol, C. Gurbuz, N. Turkelli, D. Seber and M. Barazangi, The crustal structure of the East Anatolian plateau (Turkey) from receiver functions, *Geophys. Res. Lett.* 30 (24) (2003), p. 8044.

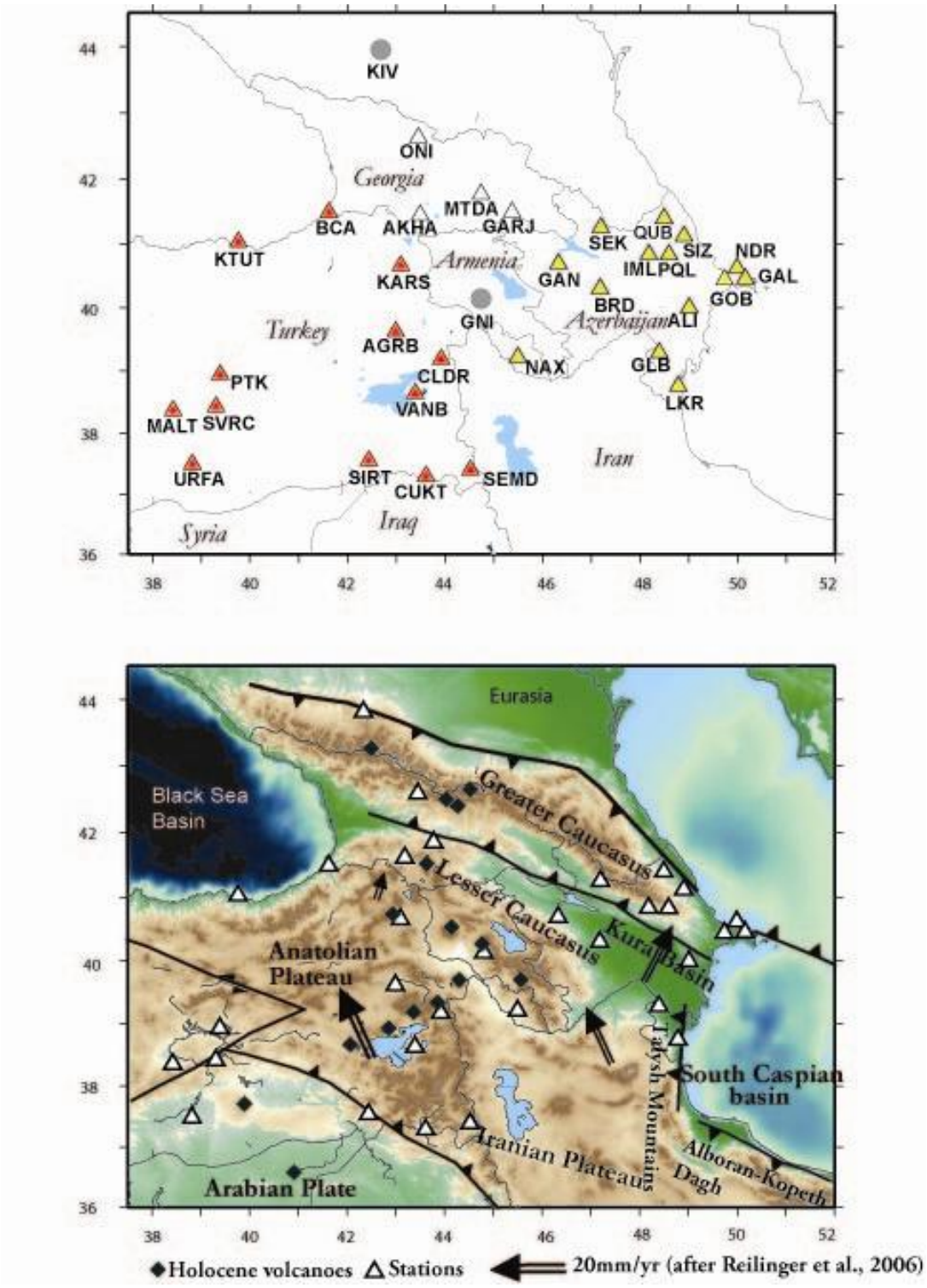

Figure 1 Stations that contributed this study with the data. Stations are color-coded with their belonging countries (Turkey:red,Georgia:white,Azerbaijan:yellow.gray circles:GSN stations). Broad-band stations include STS-2, ESP3T, ESP3ESD and CMG40T type instruments.

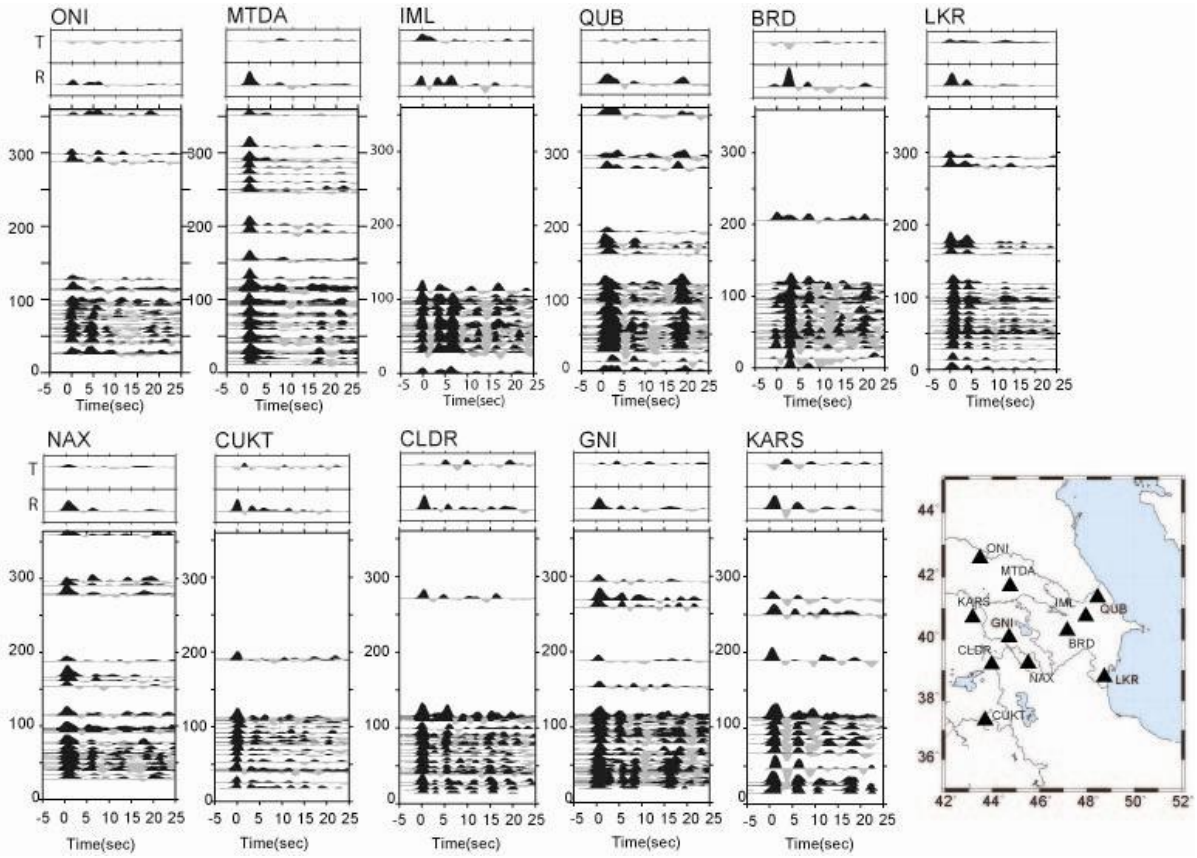

Figure 2 Receiver functions (filtered with a Gaussian filter width of 1.0 second) plotted as a function of backazimuth from selected stations in the region. The stacked traces of radial(R) and transverse (T) receiver functions are shown on top of each panel.

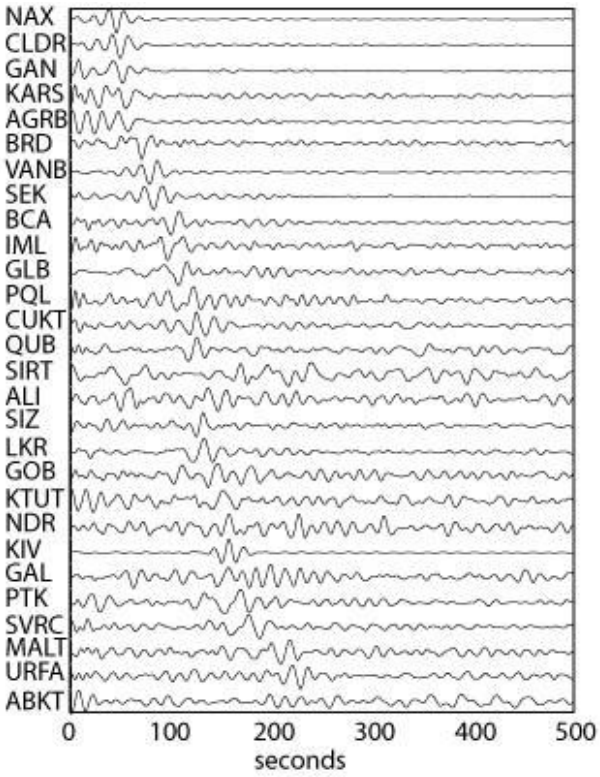

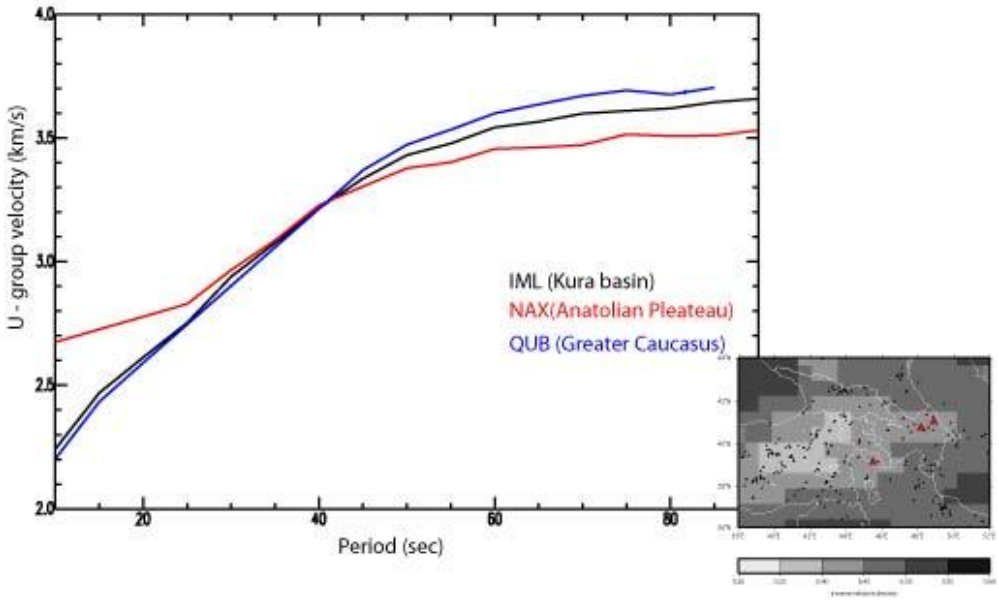

Figure 3 a) Ambient-noise correlation results of GNI with the rest of stations, filtered at 20-50 sec. **b)** Example of surface-wave dispersion curves extracted from the regional/global tomography map after including data from this study. The ray density map shown at lower right (with highlighted station locations shown on the graph)

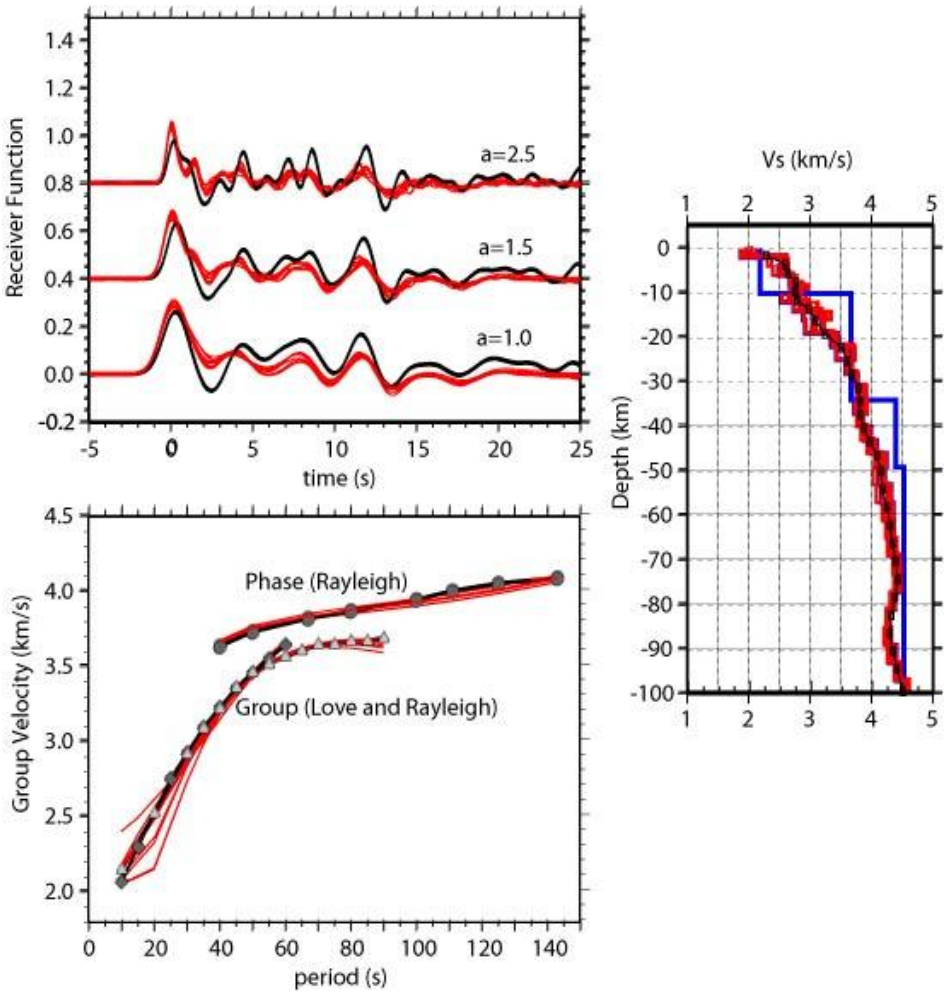

Figure 4 An example of how the joint inversion is performed with combined measurements. Note that the Love and Rayleigh waves are completely overlapped between10-50sec. Blue is the starting model on the right panel. Red line is synthetic.

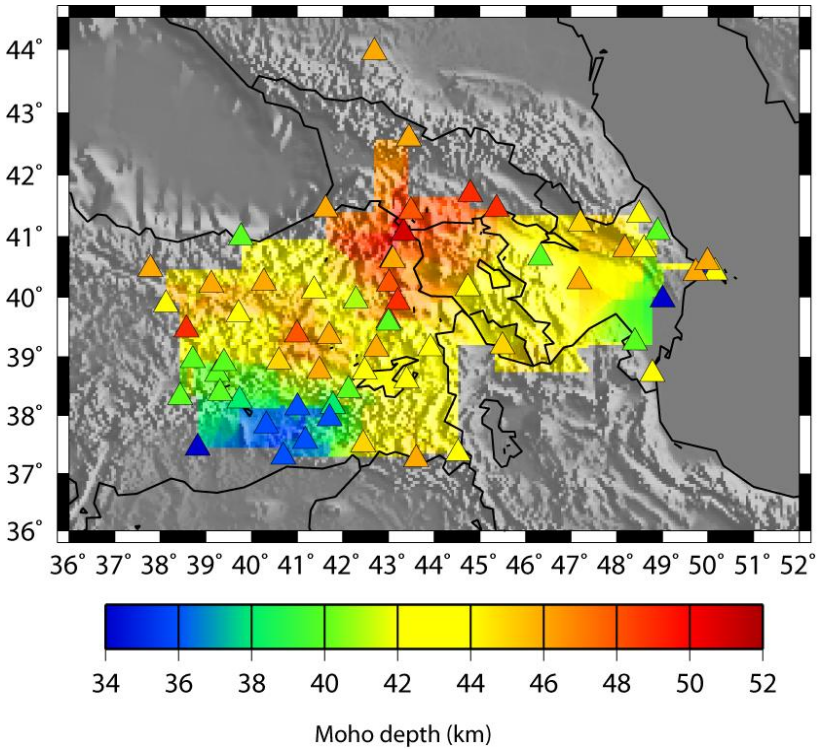

Figure 5 The figure of interpolated Moho depth including Moho depth results from ETSE network (Gok et al., 2003). The deepest Moho is observed in Lesser Caucasus region and the shallowest is in Arabian Plate.

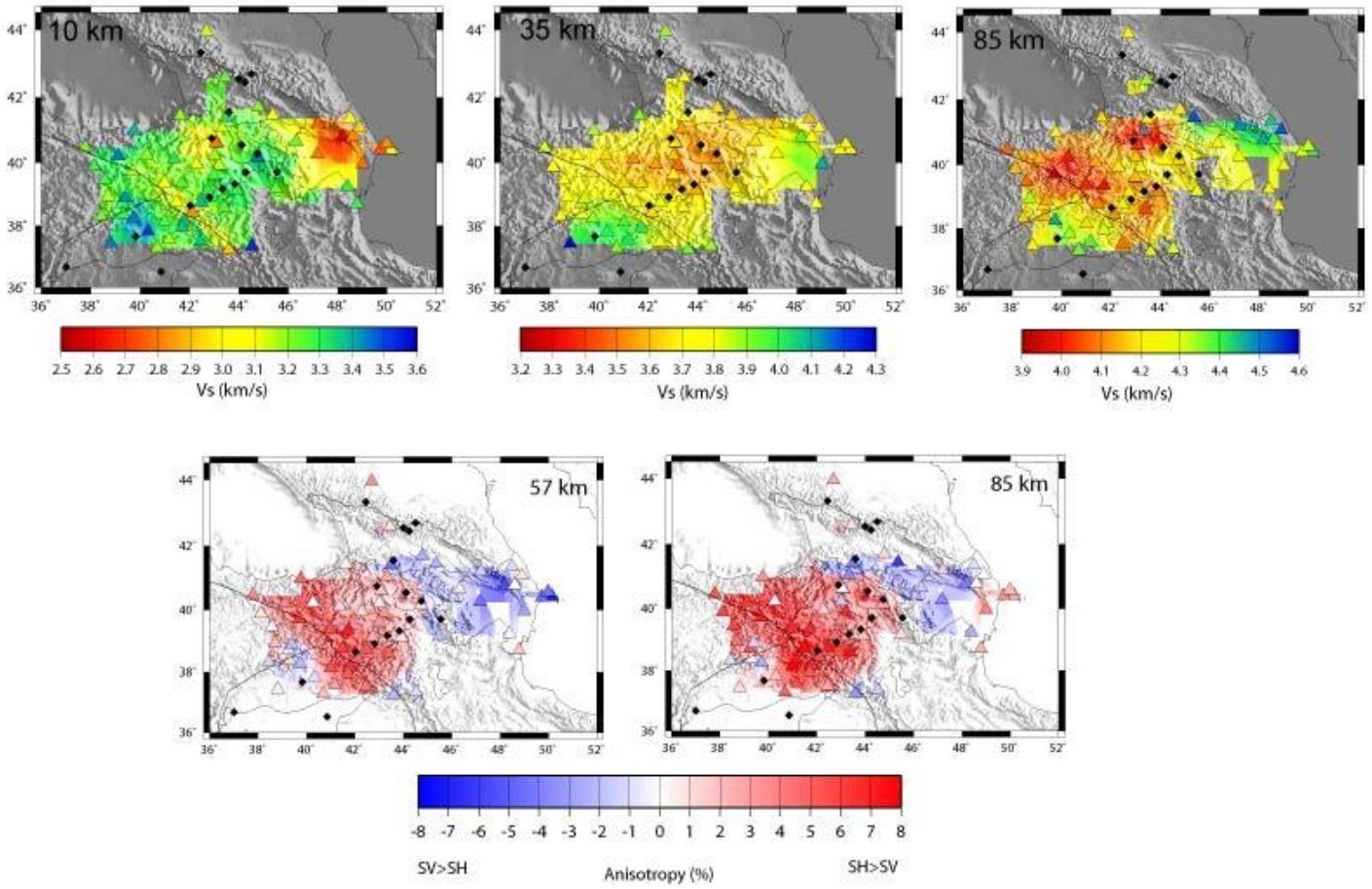

Figure 6 Horizontal slices of velocities at upper (10km), lower crust (35km) and upper mantle (85km). Thick sediments of Kura basin are still prominent at 10km depth. Slowest velocities are observed in northeastern Arabian Plateau and Lesser Caucasus. The lower crust in the Kura basin is relatively fast. Anisotropy at 57 and 85 km depth are shown on the lower panel.

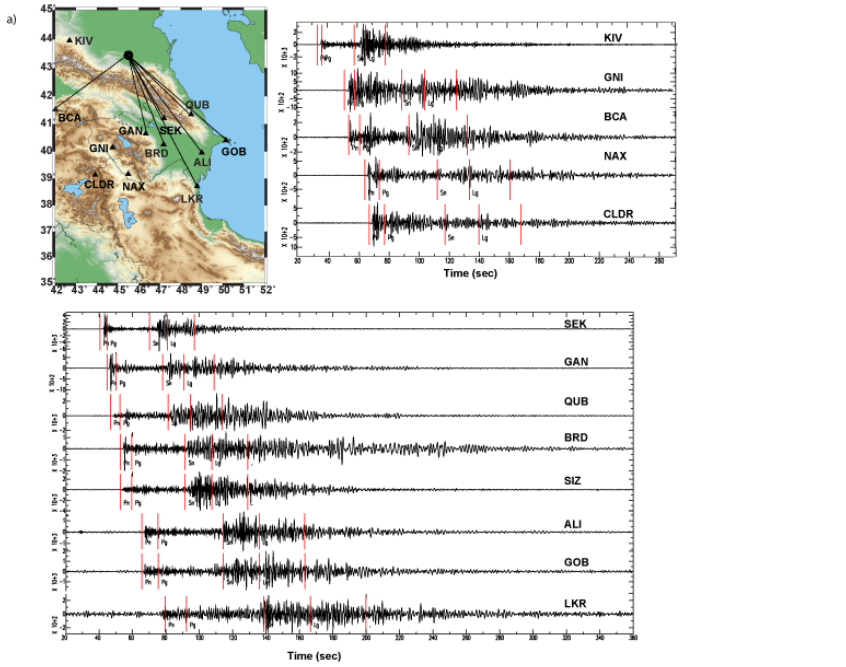

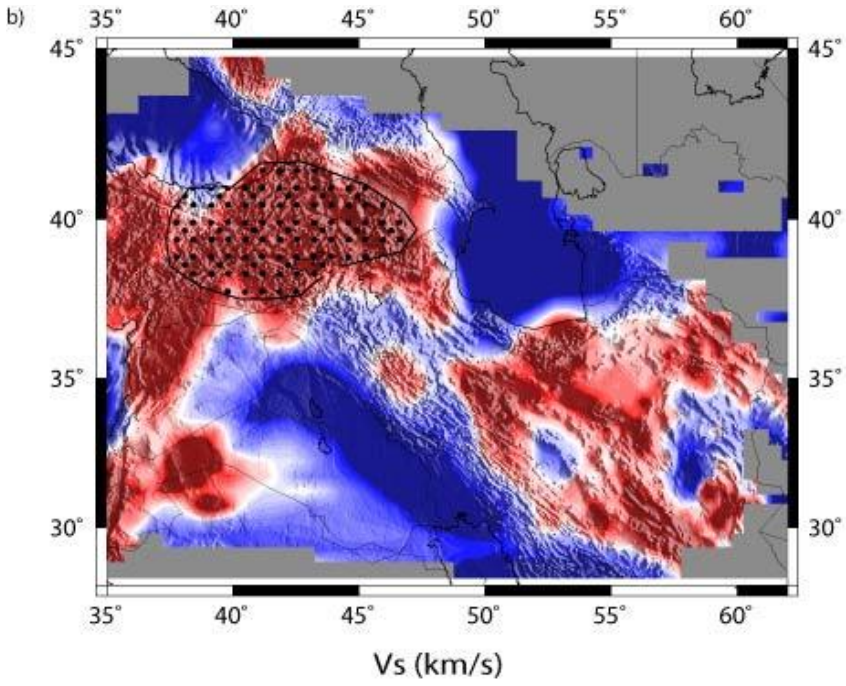

Figure 7 Sn propagation efficiency tomography. Red is blocked Sn and blue is efficiently propagating Sn. The shaded area is the low velocity anomaly at 85 km (Figure 6)